Available online at www.sciencedirect.com
ScienceDirect
Journal of Sound and Vibration 305 (2007) 750–771
JOURNAL OF SOUND AND VIBRATION
www.elsevier.com/locate/jsvi

Low-dimensional maps for piecewise smooth oscillators

Ekaterina Pavlovskaia, Marian Wiercigroch*

Centre for Applied Dynamics Research, Department of Engineering, King's College, Aberdeen University, Aberdeen AB24 3UE, UK

Received 22 April 2006; received in revised form 19 April 2007; accepted 23 April 2007
Available online 2 July 2007

Abstract

Dynamics of the piecewise smooth nonlinear oscillators is considered, for which, general methodology of reducing multidimensional flows to low-dimensional maps is proposed. This includes a definition of piecewise smooth oscillator and creation of a global iterative map providing an exact solution. The global map is comprised of local maps, which are constructed in the smooth sub-regions of phase space. To construct this low-dimensional map, it is proposed to monitor the points of intersections of a chosen boundary between smooth subspaces by a trajectory. The dimension reduction is directly related to the dimension of the chosen boundary, and the lower its dimension is, the larger dimension reduction can be achieved. Full details are given for a drifting impact oscillator, where the five-dimensional flow is reduced to one-dimensional (1D) approximate analytical map. First an exact two-dimensional map has been formulated and analysed. A further reduction to 1D approximate map is introduced and discussed. Standard nonlinear dynamic analysis reveals a complex behaviour ranging from periodic oscillations to chaos, and co-existence of multiple attractors. Accuracy of the constructed maps is examined by comparing with the exact solutions for a wide range of the system parameters.

1. Introduction

Dynamics of vast majority of physical systems can be defined in terms of multidimensional flows, and if these flows are described by linear differential equations there are well-developed mathematical techniques, which can provide effective analytical solutions. However, a good deal of multidimensional flows are described by nonlinear equations, which brings difficulties in proving even the solution existence. It has been understood that the most effective way to tackle this problem is dimension reduction, and in this paper we propose a general approach to reduce dimensionality of piecewise smooth oscillators. Specifically we have shown how to create one-dimensional (1D) approximate iterative map for a piecewise linear oscillator which in autonomous form is described by five first-order differential equations.

Piecewise smooth systems are known to exhibit complex bifurcation scenarios and chaos and their dynamics has been recently intensively studied (see for example, [1]). These systems can undergo all types of bifurcations that smooth ones do, but apart from them there is whole class of bifurcations that are unique to piecewise smooth systems such as grazing [2–4], chattering [5] or sliding [6]. A good deal of work has been done to study these special bifurcations using normal form maps derived locally near grazing (see for example [6–8]).

*Corresponding author.
E-mail address: m.wiercigroch@abdn.ac.uk (M. Wiercigroch).

0022-460X/$ - see front matter © 2007 Elsevier Ltd. All rights reserved.
doi:10.1016/j.jsv.2007.04.044

The general bifurcation scenarios in explicitly defined two dimensional (2D) piecewise smooth maps were also considered in [9,10]. In the published literature there are also a number of systematic examples showing how such low-dimensional approximate maps are constructed, e.g. [2,11–13] to name a few. However, typically low-dimensional maps are constructed based on the observations of behaviour and consequently the properties of the particular systems under consideration, and the authors are not aware of any universal approach to the problem of dimension reduction. Therefore, in this article we propose a general methodology of reducing dimensionality for piecewise smooth oscillators, and we will show the process of developing first the exact 2D map and then 1D approximate map for a five-dimensional (5D) autonomous system modelling of a drifting impact oscillator.

The paper is organized as follows. In the next section general description of the non-smooth dynamical system is introduced, and a drifting impact oscillator is given as an example of 5D non-smooth system. The methodology of constructing low-dimensional maps is explained in Section 3, where the main ideas are to monitor intersections of the system trajectory with the borders of the smooth sub-regions, and to create a global map, from local maps describing the system behaviour in the individual smooth sub-regions. Again, the drifting oscillator is used to illustrate the application of general methodology. In Section 4 periodic orbits of 2D map are considered and their stability is investigated. A further reduction to 1D approximate map is introduced in Section 5, where this approximate map is also analysed. Finally, conclusions and appendixes with additional mathematical details are given.

2. Piecewise smooth dynamical systems

In many engineering applications, characteristics of a dynamical system can be non-smooth in nature, which mathematically leads to so-called piecewise smooth dynamical systems. As well-known examples, one may point out an impact oscillator (e.g. [14]), piecewise linear oscillators (e.g. [15–18]), mechanical "bouncing ball" system [19], Jeffcott rotor with bearing clearances [20–22], systems with Coulomb friction (e.g. [23,24]), gear-box systems [25–27] and metal cutting processes [28,29]. General methodology of describing and solving non-smooth dynamical system which originates from the Fillipov's approach [30] can be found for example in [31,32]. It includes modelling of discontinuous systems by discontinuous functions and by smooth functions. In this paper the first approach will be adopted, where a dynamical system is defined in global hyperspace Ω as continuous but not necessarily smooth autonomous system

$$\dot{\mathbf{x}} = \mathbf{f}(\mathbf{x}, \mathbf{p}), \tag{1}$$

where $\mathbf{x} = [x_1, x_2, \ldots, x_n]^{\mathrm{T}}$ is the state space vector (x_n is used to represent time), $\mathbf{p} = [p_1, p_2, \ldots, p_m]^{\mathrm{T}}$ is a vector of the system parameters, and $\mathbf{f}(\mathbf{x}, \mathbf{p}) = [f_1, f_2, \ldots, f_n]^{\mathrm{T}}$ is the vector function which is dependent upon the system structure or the process being modelled. Then it is assumed that the dynamical system (1) is smooth but only within a subspace $\mathbf{X}_i$ of the global hyperspace Ω (see Fig. 1). Therefore for each subspace $\mathbf{X}_i$ ($\mathbf{x} \in \mathbf{X}_i$) the right-hand side of Eq. (1) may be described by different function, $\mathbf{f}_i(\mathbf{x}, \mathbf{p})$ where $i \in [1, N]$. The global solution is obtained by matching the local solutions on the hypersurfaces $\Pi\mathbf{X}_{i,i+1}$ (where $i \in [1, N-1]$). As the system dynamics evolves, a trajectory passes through neighbouring subspaces. If the trajectory closes as shown in Fig. 1, the system exhibits periodicity which is central to the proposed scheme. Otherwise chaotic, unstable or quasiperiodic motion can occur. When a hypersurface $\Pi\mathbf{X}_{i+1,i+2}$ is intersected by a trajectory emanating from the subspace $\mathbf{X}_{i+2}$ towards $\mathbf{X}_{i+1}$ for the kth non-smoothness occurrence, the mapping $\mathbf{x}^k_{(+)} \longrightarrow \mathbf{x}^k_{(-)}$ takes place. In order to solve the system (1) with piecewise smooth forcing functions, the precise values of the crossing times t^k have to be determined as the system response may be very sensitive to any inaccuracy of the computed solutions at all non-smoothness occurrences. Consequently, suitable switch functions for the non-smoothness detection have to be formulated.

In this study we will explain the proposed reduction scheme using an example of a 5D non-smooth dynamical system, which models a drifting impact oscillator. This system has been a subject of significant studies elsewhere [18,33–35]. However, for the purpose of clarity we will briefly summarise its main features. We consider a drifting two degrees-of-freedom oscillator, i.e. a mass m is driven by an external force f containing static b and dynamic $a\cos(\omega\tau + \varphi)$ components which collides with the weightless slider having a linear visco-elastic pair of stiffness k and damping c. The system is non-dimensionalized, where τ, 2ξ, f, b, a,

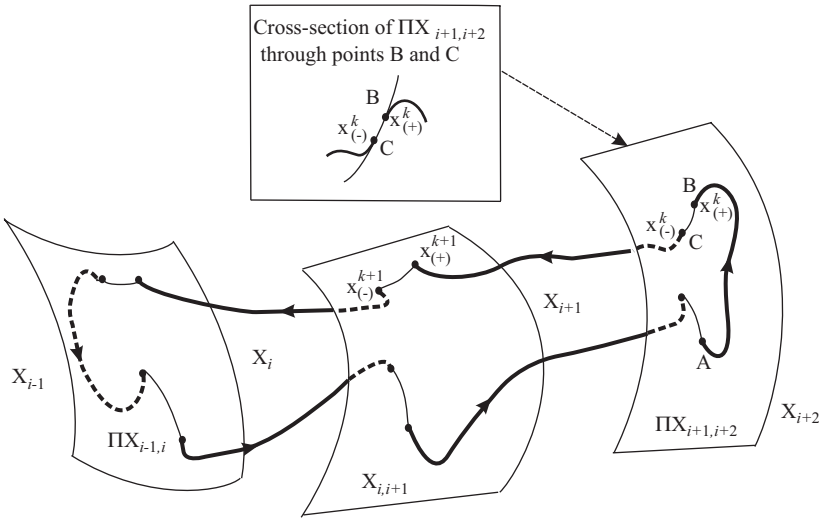

Fig. 1. Conceptual model of a piecewise smooth dynamical system, where thick lines (solid and dash) denote trajectories within subspaces and thin lines—trajectories sliding on the hypersurfaces.

and ω are non-dimensional time, damping coefficient, force, static component, and amplitude and frequency of dynamic component, respectively. As has been reported by Pavlovskaia et al. [18] the slider drifts in stick–slip phases where the relative oscillations between the mass and the slider are bounded and range from periodic to chaotic. The progressive motion of the mass occurs when the force acting on the slider exceeds the threshold of the dry friction force *d*. x, z, v represent the absolute displacements of the mass, slider top and slider bottom, respectively. It is assumed that the model operates in a horizontal plane, or the gravitational force is appropriately compensated. At the initial moment $\tau = 0$ there is a distance between the mass and the slider top called gap, e. The difference $u = (z + e) - x$ is introduced to monitor the actual distance between the mass and the slider top. For the simplicity of the further analysis the dimensionless friction threshold force, d is set to 1.

The considered system can be at the time in one of the three following modes: *No contact* (the state space vector belongs to subspace $\mathbf{X}_1$), *Contact without progression* (the state space vector belongs to subspace $\mathbf{X}_2$), and *Contact with progression* (the state space vector belongs to subspace $\mathbf{X}_3$). If the u is greater than zero, $z + e - x > 0$, then the mass and the slider top move separately during *No contact* mode. Once u is equal to zero, i.e. $z + e - x = 0$, and the force acting on the mass from the slider is greater than zero but smaller than the threshold of the dry friction force, *Contact without progression* mode occurs when the mass and the slider top move together without progression. When $u = z + e - x = 0$, and the force acting on the mass is greater than the threshold of dry friction force, then system operates in *Contact with progression* mode, where the mass and the top and the bottom of the slider move together, and progression takes place. A detailed consideration of these modes and the dimensional form of equations of motion can be found in [18]. The equations of motion are given by the following set of equations:

$$\begin{aligned} x' &= y, \\ y' &= a\cos(s + \varphi) + b - P_1P_2(1 - P_3)(2\xi y + z - v) - P_1P_3, \\ z' &= P_1 y - (1 - P_1)(z - v)/2\xi, \\ v' &= P_1P_3P_4(y + (z - v - 1)/2\xi), \\ s' &= \omega, \end{aligned} \tag{2}$$

where $P_1 = H(x - z - e)$, $P_2 = H(2\xi y + z)$, $P_3 = H(2\xi + z - 1)$, $P_4 = H(y)$, $s = \omega\tau$, $H(\cdot)$ is Heaviside step function.

As it was reported in [34] by introducing a new system of coordinates (p, q, v) instead of (x, z, v), where $p = x - v$ and $q = z - v$, it is possible to separate the oscillatory motion from the drift. In fact, in the new coordinates system p and q are displacements of the mass and the slider top relative to the current position of the slider bottom v. The equations of motion in new coordinates are given below:

$$\begin{aligned} p' &= y(1 - \mathscr{H}_3) - \frac{1}{2\xi}(q-1)\mathscr{H}_1\mathscr{H}_3\mathscr{H}_4, \\ y' &= a\cos(s+\varphi) + b - (2\xi y + q)\mathscr{H}_1\mathscr{H}_2(1-\mathscr{H}_3) - \mathscr{H}_1\mathscr{H}_3\mathscr{H}_4, \\ q' &= y\mathscr{H}_1\mathscr{H}_2(1-\mathscr{H}_3) - \frac{1}{2\xi}(q-1)\mathscr{H}_1\mathscr{H}_3\mathscr{H}_4 - \frac{1}{2\xi}q(1-\mathscr{H}_1), \\ s' &= \omega, \end{aligned} \tag{3}$$

where $\mathscr{H}_1 = H(p-q-e)$, $\mathscr{H}_2 = H(2\xi y + q)$, $\mathscr{H}_3 = H(2\xi + q - 1)$, $\mathscr{H}_4 = H(y)$, $s = \omega\tau$.

The fifth equation is $v' = 0$ during *No contact* and *Contact without progression* modes when the slider bottom remains stationary, and $v' = y + (1/2\xi)(q-1)$ during *Contact with progression* mode when the slider bottom moves with velocity v'. As can be seen from these equations, the bounded oscillations can be considered separately and drifting motion can be re-constructed thereafter.

The equations of motion are linear for each mode, therefore the global solution can be constructed by joining the local solutions at the points of non-smoothness. The set of initial values $(\tau_0; p_0, y_0, q_0)$ defines in which mode the system will operate. If $p_0 < q_0 + e$, it will be *No contact* mode. For $p_0 = q_0 + e$, it will be *Contact without progression* mode if $0 < 2\xi y_0 + q_0 < 1$ or *Contact with progression* mode if $2\xi y_0 + q_0 \geqslant 1$. The solutions for all specified modes are given in Appendix A. When the conditions corresponding to the current mode fail, the next mode begins. The final displacements and velocity for the preceding mode define the initial conditions for the next one. All details of the semi-analytical method allowing to calculate the responses of the system using this method are given in [33].

As was mentioned earlier, the progression $v(\tau)$ can be calculated separately if the dynamics of the bounded system (p, y, q) is known (i.e. the sequence of the modes and the initial conditions for them). Since during the *No contact* and the *Contact without progression* modes the progression does not change its value, so

$$v(\tau) = v_0. \tag{4}$$

For the *Contact with progression* mode $v(\tau)$ can be calculated as

$$\begin{aligned} v(\tau) = v_0 + p_0 - e - 1 - (p_0 - e - 1)\exp\left(-\frac{\tau-\tau_0}{2\xi}\right) + y_0(\tau-\tau_0) + \frac{b-1}{2}(\tau-\tau_0)^2 \\ - \frac{a}{\omega^2}[\cos(\omega\tau+\varphi) - \cos(\omega\tau_0+\varphi) + \omega(\tau-\tau_0)\sin(\omega\tau_0+\varphi)]. \end{aligned} \tag{5}$$

3. Construction of low-dimensional maps

In this section general methodology of reducing multidimensional flows to low-dimensional iterative maps for the piecewise oscillators is given. Poincaré return map is a standard method of constructing maps for both smooth and discontinuous dynamical systems, however it allows to reduce system dimension only by 1. Another common method of constructing maps is related to rigid impacts where velocity after impact is modelled by a coefficient of restitution (see for example [36–39]).

There have been a number of successful attempts in the past to reduce the system dimensionality by creating approximate low-dimensional maps. For example, Lorenz [40] constructed 1D approximate map for 3D system of ODEs describing a simple model of convection in the atmosphere. Ikeda [41] created an approximate map to study dynamics of a laser pulse in an optical cavity. Wiesenfeld and Tufillaro [19] constructed an approximate map for the bouncing ball problem using a high-bounce approximation. Nordmark [2] derived an approximate map near grazing to study changes of periodic responses for an impact oscillator. Banerjee et al. [11,12] considered power electronic circuits and obtained low-dimensional maps for different DC–DC converters by observing the state vector at every clock instant. However in all these and

others cases, properties of the particular systems have been used, and no universal approach to the problem of dimension reduction has been offered.

The approached proposed in this paper was inspired by the ideas formulated in the earlier work on impact maps (see for example [15,36–39]). The technique of constructing a map on the rigid impact surface is generalised here for piecewise smooth systems with a number of discontinuous boundaries, which are not limited anymore to the rigid constrains. To construct a low-dimensional map, it is proposed to monitor the points of intersections of a chosen boundary (hypersurface $\Pi\mathbf{X}_{i,i+1}$ shown in Fig. 1) by the trajectory. In this case, the reduction of dimension is directly related to the dimension of the chosen hypersurface, and the lower its dimension is, the larger dimension reduction can be achieved.

The following procedure is proposed to construct global low-dimensional map for the piecewise smooth dynamical system. First, the hypersurface $\Pi\mathbf{X}_{j,j+1}$ with the lowest dimension has to be chosen as the reference hypersurface. Then the local maps in each of smooth subspaces $\mathbf{X}_i$ of the global hyperspace Ω have to be constructed. For each smooth subspace $\mathbf{X}_i$ local maps will map the points belonging to initial boundary hypersurface ($\Pi\mathbf{X}_{i,i+1}$ or $\Pi\mathbf{X}_{i-1,i}$) to the "destination" boundary hypersurface, which is again $\Pi\mathbf{X}_{i,i+1}$ or $\Pi\mathbf{X}_{i-1,i}$. It should be noted that depending on the system, more than one local map can exist for each subspace, for example, mapping $\Pi\mathbf{X}_{i-1,i}$ to $\Pi\mathbf{X}_{i,i+1}$, or mapping $\Pi\mathbf{X}_{i,i+1}$ to $\Pi\mathbf{X}_{i-1,i}$, or mapping $\Pi\mathbf{X}_{i-1,i}$ to $\Pi\mathbf{X}_{i-1,i}$. The next step is to define local maps on the each hypersurface $\Pi\mathbf{X}_{i,i+1}$ ($i \in [1, N-1]$), which will map the initial position of the system on this hypersurface to the final position $\mathbf{x}^k_{(+)} \longrightarrow \mathbf{x}^k_{(-)}$ (see Fig. 1). For an impact oscillator making contact with the rigid boundary, the direction of the mass velocity will instantly change at the moment of impact, and this has to be described by the local map introduced on the hypersurface. Once all local maps are defined, the global map can be constructed by matching local solutions. Thus the global map monitors only points on the chosen hypersurface $\Pi\mathbf{X}_{j,j+1}$, and this can be achieved by starting from the point on $\Pi\mathbf{X}_{j,j+1}$ and then following the sequence of local maps (which is *a priori* unknown) until the hypersurface $\Pi\mathbf{X}_{j,j+1}$ will be intersected by the trajectory again. The implementation of this procedure is presented below for the impact oscillator with drift defined in Section 2.

The four-dimensional (4D) flow of this system $(\tau; p, y, q)$ can be locally three dimensional (3D) as during the contact modes relative displacements of the mass and slider top are not independent, i.e. $p = q + e$. This means that subspaces $\mathbf{X}_2$ and $\mathbf{X}_3$ are in fact 3D hypersurfaces, and consequently the borders $\Pi\mathbf{X}_{1,2}$, $\Pi\mathbf{X}_{2,3}$, $\Pi\mathbf{X}_{3,2}$ and $\Pi\mathbf{X}_{2,1}$ are 2D. The intersections of the trajectories with these borders allow to define a 2D map. Similarly to Luo and Menon [42] the borders of the different modes of the system are given as:

$$\begin{aligned}
&\Pi\mathbf{X}_{1,2} \equiv \Sigma_1 = \{(\tau_i; p_i, y_i, q_i) |\ p_i = e,\ y_i > 0,\ q_i = 0\},\\
&\Pi\mathbf{X}_{2,3} \equiv \Sigma_2 = \{(\tau_i; p_i, y_i, q_i) |\ p_i = 1 + e - 2\xi y_i,\ y_i > 0,\ q_i = 1 - 2\xi y_i\},\\
&\Pi\mathbf{X}_{3,2} \equiv \Sigma_3 = \{(\tau_i; p_i, y_i, q_i) |\ p_i = 1 + e - 2\xi y_i,\ y_i < 0,\ q_i = 1 - 2\xi y_i\},\\
&\Pi\mathbf{X}_{2,1} \equiv \Sigma_4 = \{(\tau_i; p_i, y_i, q_i) |\ p_i = e - 2\xi y_i,\ y_i < 0,\ q_i = -2\xi y_i\}.
\end{aligned} \tag{6}$$

These subspaces and hypersurfaces are shown in Fig. 2a. The borders of the different modes (2D hypersurfaces) are represented by lines Σ_1, Σ_2, Σ_3 and Σ_4. As can be seen from Fig. 2b during *No contact* mode (i.e. the space vector belongs to subspace $\mathbf{X}_1$), the trajectory lies in vicinity of the horizontal plane, $q = 0$, and during *Contact without progression* and *Contact with progression* modes it belongs to the inclined plane, $q = p - e$ (i.e. degenerated subspaces $\mathbf{X}_2$ and $\mathbf{X}_3$).

Based on the four hypersurfaces (6), six local maps (see Fig. 3a) can be defined as follows:

$$\begin{aligned}
&\mathbf{P}_1: \Sigma_1 \to \Sigma_2, \quad \mathbf{P}_2: \Sigma_2 \to \Sigma_3, \quad \mathbf{P}_3: \Sigma_3 \to \Sigma_4,\\
&\mathbf{P}_4: \Sigma_4 \to \Sigma_1, \quad \mathbf{P}_5: \Sigma_1 \to \Sigma_4, \quad \mathbf{P}_6: \Sigma_3 \to \Sigma_2.
\end{aligned} \tag{7}$$

As trajectory of the considered system never slides on the boundary hypersurfaces, there are no local maps on the hypersurfaces, and the global map $\mathbf{P}$ composed only from local maps in subspaces can be introduced. To construct an iterative map a hypersurface with the lowest dimension has to be chosen. For the considered oscillator it appears that all boundaries defined in Eq. (6) have the same dimension allowing to define a 2D map, where the state of the system is fully described by a new variable $\psi = \omega\tau + \varphi$ and velocity y at the moment of intersection τ_n. As velocity in the beginning of the *Contact with progression* mode could provide a good indication for the length of this mode and finally the level of the progression achieved by the oscillator,

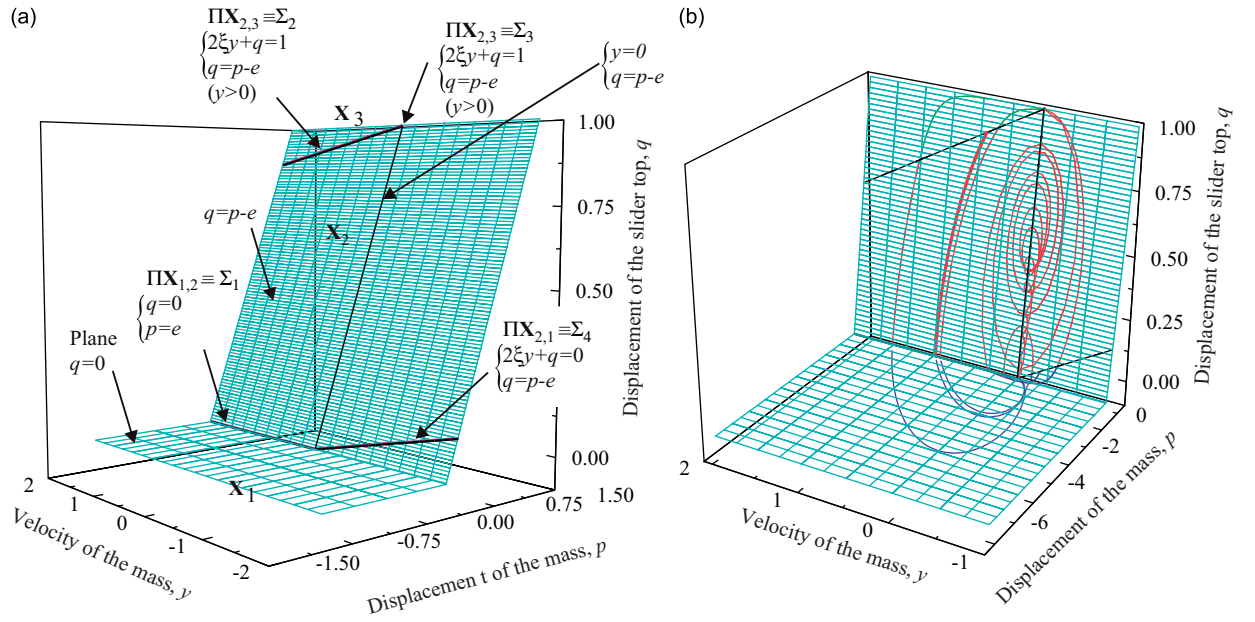

Fig. 2. (a) The concept of subspaces ($\mathbf{X}_1$,$\mathbf{X}_2$,$\mathbf{X}_3$) and hypersurfaces ($\Pi\mathbf{X}_{1,2}$, $\Pi\mathbf{X}_{2,3}$, $\Pi\mathbf{X}_{3,2}$, $\Pi\mathbf{X}_{2,1}$) applied to the system (3) and drawn in 3D, (b) trajectory of the system calculated for $a = 0.3,\ b = 0.265,\ \xi = 0.03,\ \omega = 0.1,\ \varphi = 0,\ e = 0.2$.

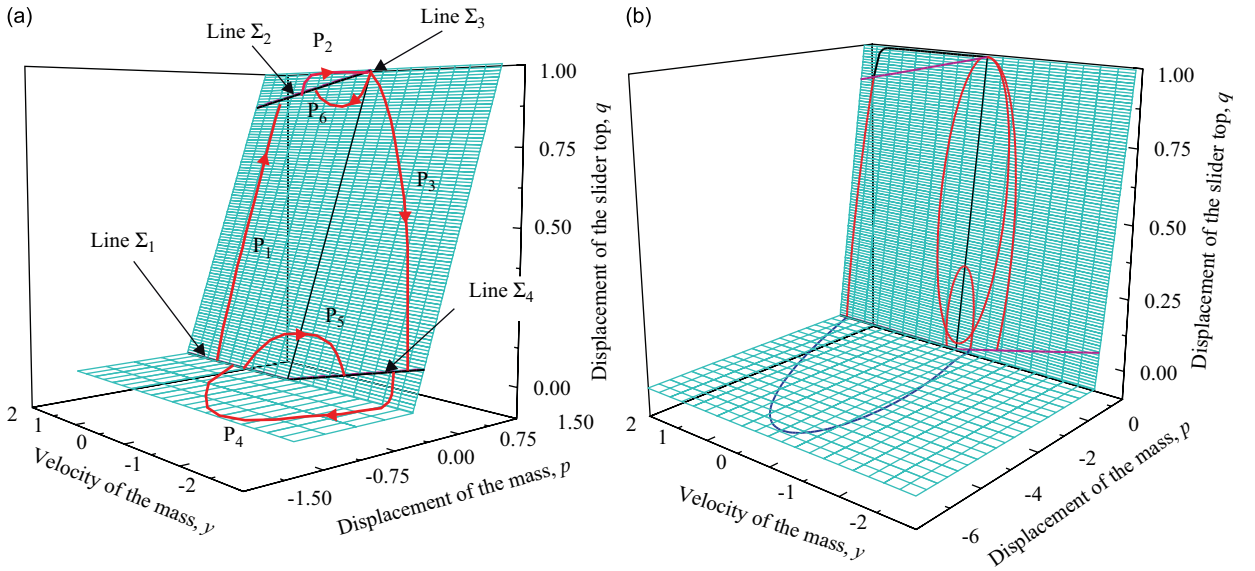

Fig. 3. (a) Symbolic representation of local maps and (b) trajectory calculated for $a = 0.3,\ b = 0.26,\ \xi = 0.03,\ \omega = 0.1,\ \varphi = 0,\ e = 0.2$.

the border $\Pi\mathbf{X}_{2,3}$ has been chosen to construct a global 2D map

$$\mathbf{P}: \Sigma_2 \to \Sigma_2, \tag{8}$$

which maps velocity y and $\psi = \omega\tau + \varphi$ at the beginning of the *Contact with progression* mode to themselves, $(y_{n+1}, \psi_{n+1}) = \mathbf{P}(y_n, \psi_n)$ (see [35]). Map $\mathbf{P}$ is an unknown combination of the local maps; and it can be equal to $\mathbf{P} = \mathbf{P}_1 \circ \mathbf{P}_4 \circ \mathbf{P}_3 \circ \mathbf{P}_2$, $\mathbf{P} = \mathbf{P}_6 \circ \mathbf{P}_2$ or $\mathbf{P} = \mathbf{P}_1 \circ \mathbf{P}_4 \circ \mathbf{P}_5 \circ \mathbf{P}_4 \circ \mathbf{P}_3 \circ \mathbf{P}_2$ or another combination of local maps.

For the harmonic external force the introduced 2D map is defined in the bounded region $\psi_n \in (0, 2\pi)$, $y_n \in (0, y^{\max})$, where $y^{\max}$ was estimated in [35].

4. Fixed points of two-dimensional map

Let us consider one of the simplest global periodic motion, shown in Fig. 4. It corresponds to a fix point of a 2D mapping which maps the beginning of *Contact without progression* mode to itself, $\Sigma_1 \to \Sigma_1$. We investigate two specific maps, $\hat{\mathbf{P}}$ and $\check{\mathbf{P}}$ describing period 1 and 2 motion. Map $\hat{\mathbf{P}}$ is the following combination of the local maps,

$$\hat{\mathbf{P}} = \mathbf{P}_4 \circ \mathbf{P}_3 \circ \mathbf{P}_2 \circ \mathbf{P}_1. \tag{9}$$

Based on Eq. (9) for $(\tau_i, y_i) \in \Sigma_1$ the mapping route is

$$\begin{aligned}
&\mathbf{P}_1: (\tau_i, y_i) \to (\tau_{i+1}, y_{i+1}),\\
&\mathbf{P}_2: (\tau_{i+1}, y_{i+1}) \to (\tau_{i+2}, y_{i+2}),\\
&\mathbf{P}_3: (\tau_{i+2}, y_{i+2}) \to (\tau_{i+3}, y_{i+3}),\\
&\mathbf{P}_4: (\tau_{i+3}, y_{i+3}) \to (\tau_{i+4}, y_{i+4}),
\end{aligned}$$

which results in the global map

$$\hat{\mathbf{P}}: (\tau_i, y_i) \to (\tau_{i+4}, y_{i+4}). \tag{10}$$

Periodicity conditions for period one motion are

$$\tau_{i+4} = \tau_i + T \quad \text{and} \quad y_{i+4} = y_i, \tag{11}$$

where $T = 2\pi/\omega$ is a period of the external excitation.

The fixed points of the map (9) can be found analytically and their stability can be examined as the behaviour of the system is described by linear ODEs in each smooth subspace. To do this the exact solutions

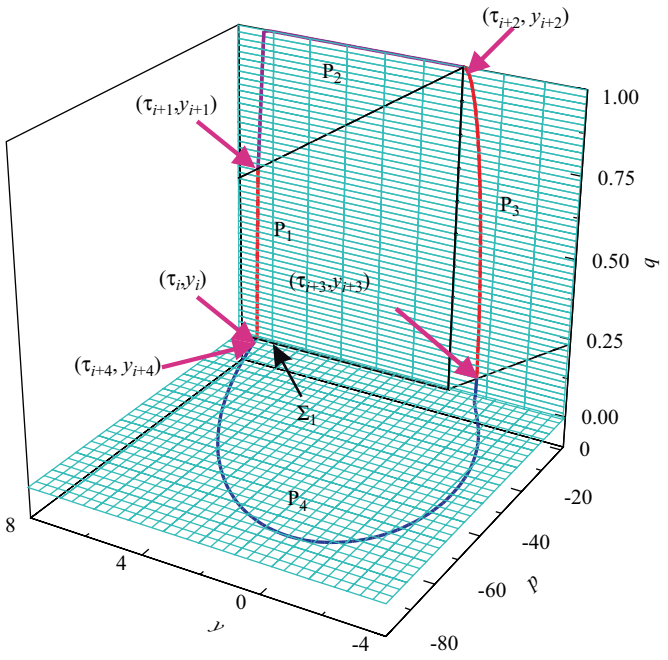

Fig. 4. Global map $\hat{\mathbf{P}}$ developed for period one regime existing for the following values of parameters $a = 0.3, b = 0.15, \xi = 0.03, \omega = 0.1, \varphi = 0, e = 0.2$.

given in Appendix A and numerical calculations of the intersections times τ_{n+1}, τ_{n+2}, τ_{n+3} and τ_{n+4} were used and the procedure is described below.

The mapping $\mathbf{P}_1$ associates the initial moment of *Contact without progression* mode with initial moment of *Contact with progression* mode. To find τ_{i+1} implicit equation $\mathcal{G}_1(\tau_{i+1}) = 2\xi y(\tau_{i+1}) + p(\tau_{i+1}) - e - 1 = 0$, has to be solved, where functions $y(\cdot)$ and $p(\cdot)$ are given in Eq. (23):

$$\begin{aligned}\mathcal{G}_1(\tau_{i+1}) = b &+ \exp(-\xi(\tau_{i+1}-\tau_i))\sqrt{C_1^2+C_2^2}\sin\left(\sqrt{1-\xi^2}(\tau_{i+1}-\tau_i)+\beta(C_1,C_2)\right)\\ &+\frac{a}{\sqrt{(1-\omega^2)^2+4\xi^2\omega^2}}\sin(\omega\tau_{i+1}+\varphi+\alpha)\\ &+2\xi\left[\exp(-\xi(\tau_{i+1}-\tau_i))\sqrt{C_1^2+C_2^2}\sin\left(\sqrt{1-\xi^2}(\tau_{i+1}-\tau_i)+\delta(C_1,C_2)\right)\right.\\ &\left.+\frac{a\omega}{\sqrt{(1-\omega^2)^2+4\xi^2\omega^2}}\cos(\omega\tau_{i+1}+\varphi+\alpha)\right]-1=0.\end{aligned} \tag{12}$$

Coefficients C_1 and C_2 are functions of initial conditions and they are defined by Eqs. (24) and (25)

$$\begin{aligned}C_1 &= C_1(\tau_i, e),\\ C_2 &= C_2(\tau_i, e, y_i),\end{aligned} \tag{13}$$

where the formulae for $\alpha, \gamma, \beta(C_1, C_2)$ and $\delta(C_1, C_2)$ are listed in Eq. (26).

Once Eq. (12) is solved and τ_{i+1} is determined, first velocity y_{i+1} and then relative displacement p_{i+1} can be calculated from

$$\begin{aligned}y_{i+1} = &\exp(-\xi(\tau_{i+1}-\tau_i))\sqrt{C_1^2+C_2^2}\sin\left(\sqrt{1-\xi^2}(\tau_{i+1}-\tau_i)+\delta(C_1,C_2)\right)\\ &+\frac{a\omega}{\sqrt{(1-\omega^2)^2+4\xi^2\omega^2}}\cos(\omega\tau_{i+1}+\varphi+\alpha),\end{aligned} \tag{14}$$

$$p_{i+1} = 1 + e - 2\xi y_{i+1}, \tag{15}$$

where coefficients C_1, C_2 can be calculated from Eq. (13).

The mappings $\mathbf{P}_2$, $\mathbf{P}_3$ and $\mathbf{P}_4$ are constructed in an identical manner, on which details can be found in Appendix B. In Section 3 two additional local maps $\mathbf{P}_5$ and $\mathbf{P}_6$, which have not featured in current development of global map for period one motion, have been mentioned. The details on $\mathbf{P}_5$ and $\mathbf{P}_6$ can be also found in Appendix B.

Eqs. (11)–(15) and (28)–(34) allow to calculate analytically the solution. Once the analytical form of periodic solution is available, the stability can be examined by analysing the corresponding Jacobian matrix of the global map $\hat{\mathbf{P}}$. In our case from Eq. (9) the Jacobian matrix is computed by the chain rule (see e.g. [15]):

$$D\hat{\mathbf{P}} = \left[\frac{\partial(\tau_{i+4}, y_{i+4})}{\partial(\tau_i, y_i)}\right]_{(\tau_i, y_i)} = \prod_{j=1}^{4} D\mathbf{P}_j = \prod_{j=1}^{4}\left[\frac{\partial(\tau_{i+j}, y_{i+j})}{\partial(\tau_{i+j-1}, y_{i+j-1})}\right]_{(\tau_{i+j-1}, y_{i+j-1}, \tau_{i+j}, y_{i+j})}. \tag{16}$$

For each mapping $\mathbf{P}_j$, $j \in [1, 4]$ Jacobian matrix can be calculated as

$$D\mathbf{P}_j = \left[\frac{\partial(\tau_{i+j}, y_{i+j})}{\partial(\tau_{i+j-1}, y_{i+j-1})}\right]_{(\tau_{i+j-1}, y_{i+j-1})} = \begin{bmatrix}\dfrac{\partial\tau_{i+j}}{\partial\tau_{i+j-1}} & \dfrac{\partial\tau_{i+j}}{\partial y_{i+j-1}}\\ \dfrac{\partial y_{i+j}}{\partial\tau_{i+j-1}} & \dfrac{\partial y_{i+j}}{\partial y_{i+j-1}}\end{bmatrix}_{(\tau_{i+j-1}, y_{i+j-1})}. \tag{17}$$

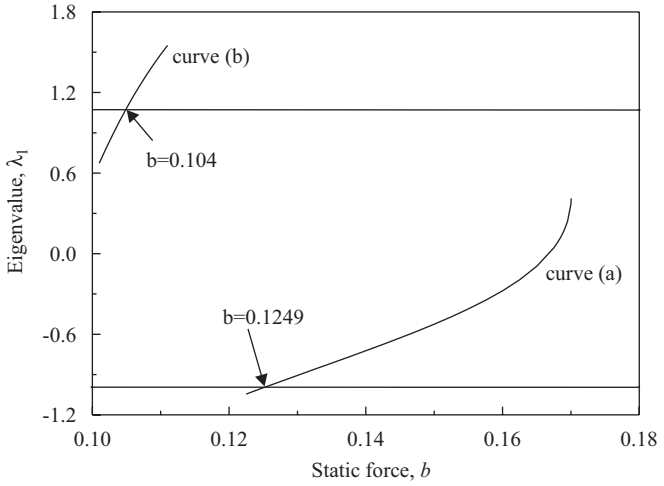

Fig. 5. Dependance of eigenvalue λ_1 on the static force b for period one and period two motions shown by curves (a) and (b) correspondingly. Both figures have been calculated for $a = 0.3$, $\xi = 0.01$, $\omega = 0.1$, $\varphi = 0$, $e = 0.02$.

Equations $\mathscr{G}_j(\tau_{i+j}) = 0$, $(j \in [1,4])$ implicitly define τ_{i+j} as functions of $(\tau_{i+j-1}, y_{i+j-1})$. Thus using implicit differentiation one can obtain partial differentials:

$$\frac{\partial \tau_{i+j}}{\partial \tau_{i+j-1}} = -\frac{\partial \mathscr{G}_j}{\partial \tau_{i+j-1}} \Big/ \frac{\partial \mathscr{G}_j}{\partial \tau_{i+j}}, \tag{18}$$

$$\frac{\partial \tau_{i+j}}{\partial y_{i+j-1}} = -\frac{\partial \mathscr{G}_j}{\partial y_{i+j-1}} \Big/ \frac{\partial \mathscr{G}_j}{\partial \tau_{i+j}}. \tag{19}$$

To obtain $(\partial y_{i+j})/(\partial \tau_{i+j-1})$ and $(\partial y_{i+j})/(\partial y_{i+j-1})$ derivatives of explicit functions (14), (29), (32) and (34) have to be used, where values of $(\partial \tau_{i+j})/(\partial \tau_{i+j-1})$ and $(\partial \tau_{i+j})/(\partial y_{i+j-1})$ are calculated using Eqs. (18) and (19). The explicit expressions for all terms of Jacobian matrices $D\mathbf{P}_j$, $j \in [1,6]$ can be found in Appendix B.

The eigenvalues of the Jacobian matrix (16) allow to study stability of period one motion by varying system parameters. These eigenvalues can be expressed as $\lambda_{1,2} = \mathrm{Re}(\lambda_{1,2}) + \imath \mathrm{Im}(\lambda_{1,2})$, where $\imath = \sqrt{-1}$. If $|\lambda_j| < 1$ for $j = 1, 2$ the solution is stable, and it is unstable otherwise. By varying system parameters the stability can be examined. Curve (a) in Fig. 5 shows a dependance of eigenvalue λ_1 on the static force b for $a = 0.3$, $\xi = 0.01$, and $\omega = 0.1$. The eigenvalue λ_2 is also a real number and it is very small in this range of b, $|\lambda_2| < 10^{-6}$. As can be seen from Fig. 5, under decreasing b λ_1 becomes smaller than -1 at $b = 0.1249$ which means that in this point period one motion losses stability and a flip period doubling bifurcation occurs. This period doubling bifurcation is clearly seen on the bifurcation diagram shown in Fig. 11b calculated also for $a = 0.3$, $\xi = 0.01$, $\omega = 0.1$.

Using the same approach the stability of period two regime with mapping $\breve{\mathbf{P}} = \mathbf{P}_4 \circ \mathbf{P}_3 \circ \mathbf{P}_2 \circ \mathbf{P}_1 \circ \mathbf{P}_4 \circ \mathbf{P}_3 \circ \mathbf{P}_2 \circ \mathbf{P}_1$ can be investigated. The dependence of the first eigenvalue λ_1 calculated for this mapping $\breve{\mathbf{P}}$ on the static force, b is shown by curve (b) in Fig. 5 indicating a difference in position of the bifurcation point for increasing (period two loses stability) and decreasing (period one loses stability) value of control parameter b. The second eigenvalue λ_2 is as before a real number $|\lambda_2| < 10^{-6}$.

Due to the fact that the second eigenvalue λ_2 is very small for all investigated system responses, an idea of further reduction of dimensionality to 1D approximate map was pursued and this will be explored in the next section.

5. One-dimensional approximate map

The detailed analysis of the considered system reveals that a further reduction to 1D approximate map is possible. It has been found that the actual positions of the system at the end of the *Contact with progression*

phase (points belonging to the hypersurface Σ_3) are very close to the point

$$\tilde{\Sigma}_3 = \{(\tau_i; p_i, y_i, q_i) | p_i = 1 + e, y_i = 0, q_i = 1\} \tag{20}$$

and therefore approximate 1D map

$$\mathscr{P}: \tilde{\Sigma}_3 \to \tilde{\Sigma}_3 \tag{21}$$

can be introduced. Relation (21) maps the variable ψ at the end of the *Contact with progression* mode to itself, $\psi_{n+1} = \mathscr{P}(\psi_n)$. The iterations of the proposed 1D approximate maps converging to period one regimes are shown in Figs. 6 and 7, and to period six and for chaotic regimes in Fig. 8. In Figs. 6a, 7a and 8b each iterative step is marked by numbers $1, 2, 3, \ldots$, whereas in Fig. 8a numbers from 1 to 6 indicate the established period six motion. As can be seen from these figures the 1D approximate maps are piecewise smooth, and they vary significantly for different values of the static force.

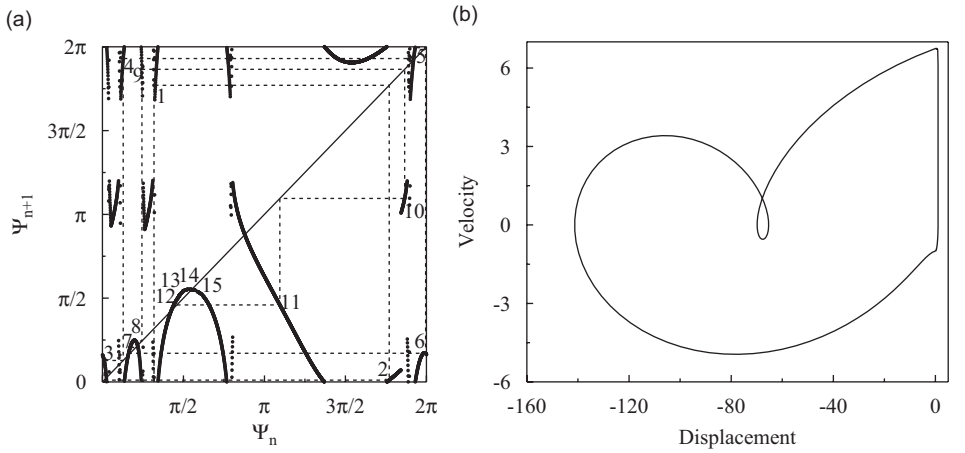

Fig. 6. (a) Iteration of 1D mapping converging to period one motion and (b) trajectory for this regime on (p, y) plane calculated at $a = 0.3$, $b = 0.07$, $\xi = 0.01$, $\omega = 0.1$, $\varphi = 0$, $g = 0.02$.

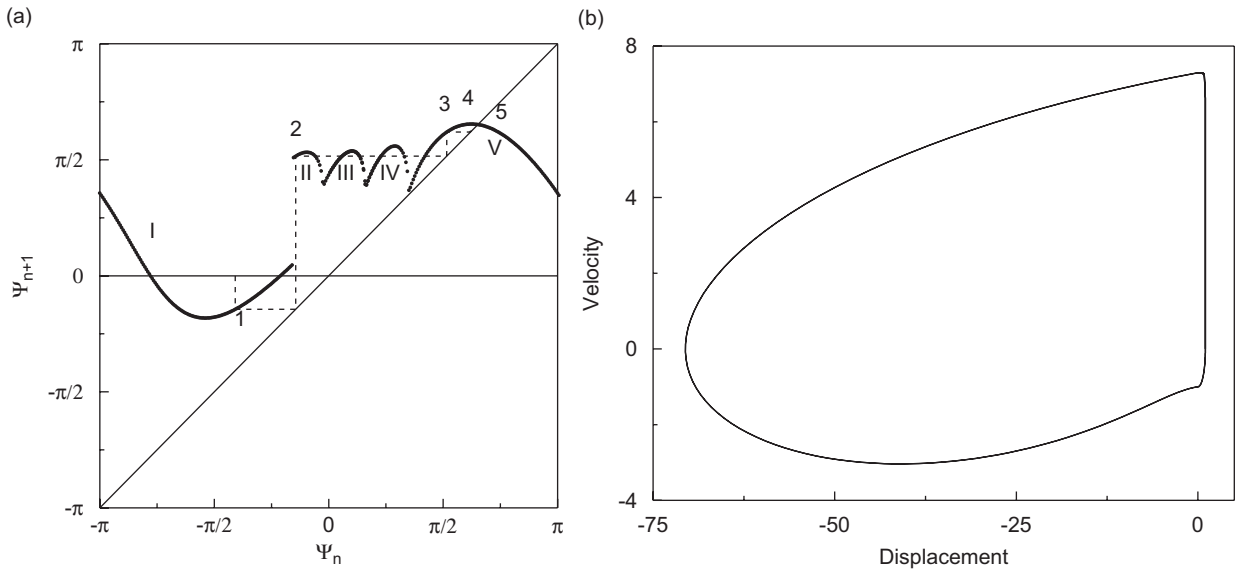

Fig. 7. (a) Iteration of 1D mapping converging to period one motion and (b) trajectory for this regime on (p, y) plane calculated at $a = 0.3$, $b = 0.15$, $\xi = 0.01$, $\omega = 0.1$, $\varphi = 0$, $g = 0.02$.

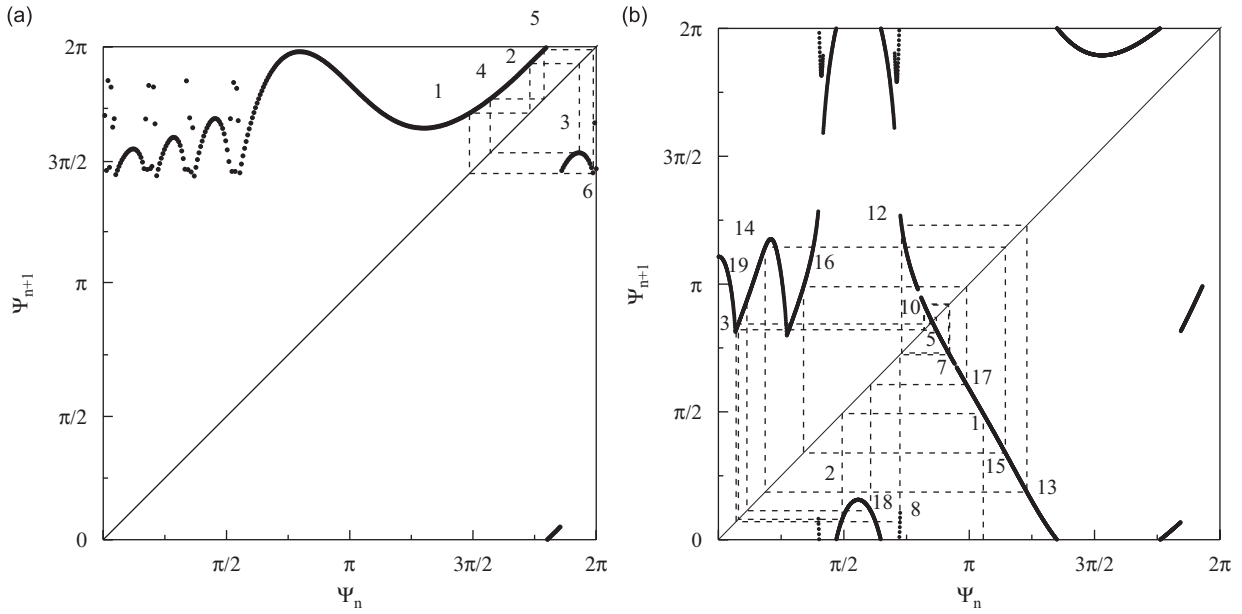

Fig. 8. Iteration of 1D mapping (a) converging to period six motion at $b = 0.29$ and (b) for chaotic regime at $b = 0.08$ for $a = 0.3$, $\xi = 0.01$, $\omega = 0.1$, $\varphi = 0$, $g = 0.02$.

Let us consider the map shown in Fig. 7a in more details. This map is presented in symmetrical region of phase shift $\psi \in (-\pi, \pi)$ and as can be seen it has five distinctive smooth sub-regions marked by numbers from I to V, where the first one is the continuation of the last one. Each of these sub-regions corresponds to different types of system behaviour between two consecutive progression phases, i.e. for each of them the actual form of the map $\mathscr{P}$ defined by a number of the *No contact* and *Contact without progression* modes is different. The behaviour of the system on the (p, y) plane during one iteration of the map for these sub-regions is shown in Figs. 9a–f. For example, the graphs in Figs. 9a and b shows how starting from any ψ_n in the first region, system will go through *Contact without progression* (marked by dash line), *No contact* (thin solid line), *Contact without progression* and *Contact with progression* (thick solid line) modes to reach ψ_{n+1}. These graphs are calculated for $\psi_n = -3$ (Fig. 9a) and for $\psi_n = -0.48$ (Fig. 9b). The last value of $\psi_n = -0.48$ is close to the second sub-region for which typical system behaviour is shown in Fig. 9c. In the first sub-region as the value of ψ_n increases, velocity of the mass hitting the slider decreases, and consequently the duration of the progression phase decreases until the system is completely de-phased and impact of the mass does not cause any progression. At this point $\psi_n = -0.499$ there is a jump on the map (Fig. 7a), and for any ψ_n which is greater than -0.499 the mass will hit the slider a number of times before it will build up energy for the next impact with progression. In the second sub-region, there are three hits without progression (see zoom-up window in Fig. 9c), in the third sub-region—two hits (Fig. 9d), in the forth sub-region—one hit (Fig. 9e), and in the fifth sub-region again none (Fig. 9f).

As was mentioned earlier for this given set of parameters ($a = 0.3$, $b = 0.15$, $\xi = 0.01$, $\omega = 0.1$, $\varphi = 0$, $g = 0.02$), the system will settle down on the periodic orbit shown in Fig. 7(b) at $\psi_n = 2.047$. The transient motion before the settling down, however, might be very different depending on the chosen initial value of ψ_n. Iteration of the 1D map starting from the chosen ψ_n shows the sequence of the involved smooth sub-regions of the map which gives understanding of the transients. For example, for the iterations 1–5 given in Fig. 7a the transient motion is comprised of one iteration without additional impacts (this is marked by number 1 in Fig. 7a), one iteration with three additional impacts (number 2) and finally 2 iterations without additional impacts (numbers 3 and 4). This can be also seen from time history given in Fig. 10b, where the time moments used for map construction marked by numbers from 1 to 6. Also it can be seen that the durations of each map iteration might be different.

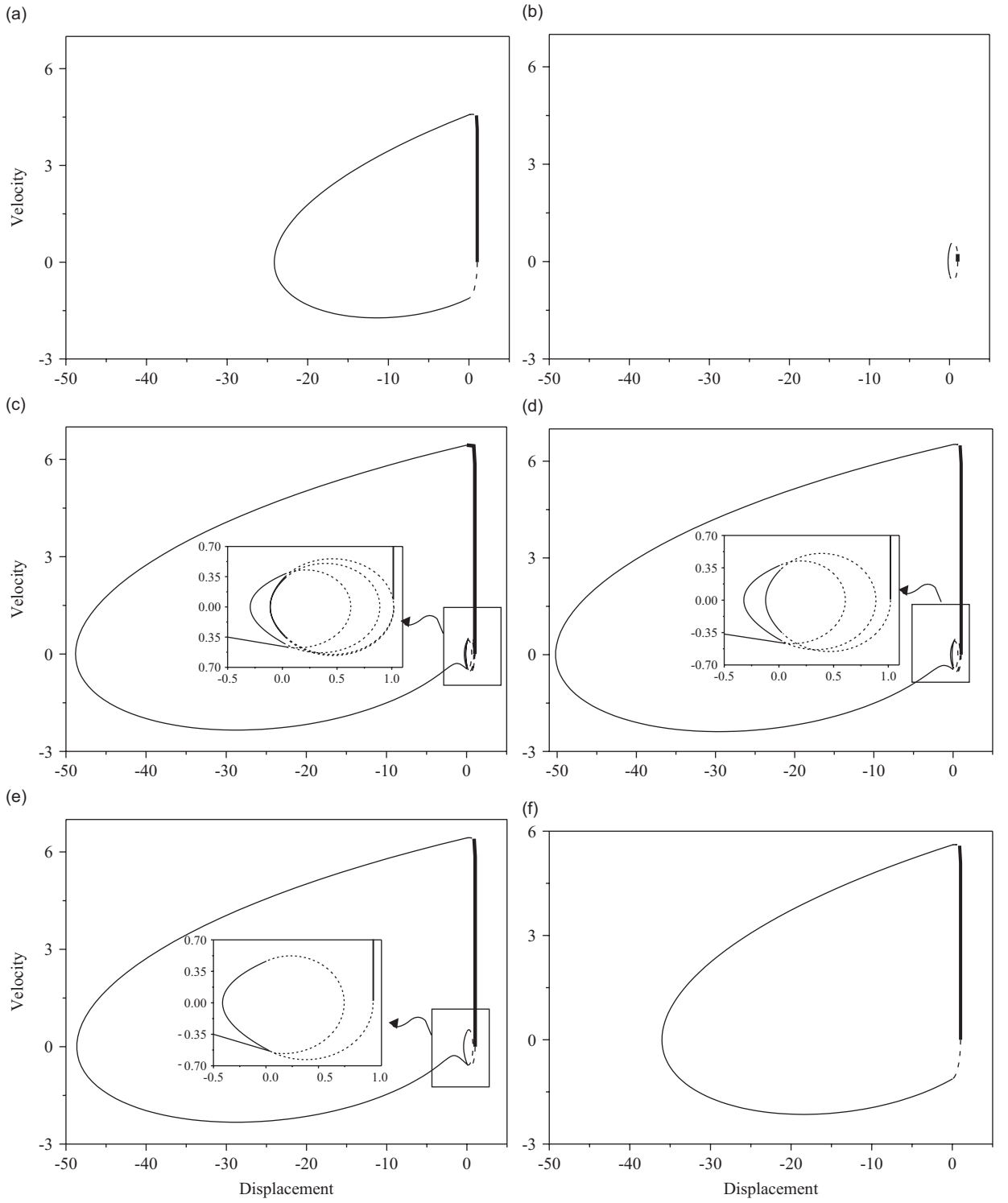

Fig. 9. Behaviour of the system during one map iteration on (p, y) plane for (a) $\psi_n = -3$, (b) $\psi_n = -0.48$, (c) $\psi_n = -0.7$, (d) $\psi_n = 0.2$, (e) $\psi_n = 0.7$ and (f) $\psi_n = 3$ at $a = 0.3$, $b = 0.15$, $\xi = 0.01$, $\omega = 0.1$, $\varphi = 0$, $g = 0.02$.

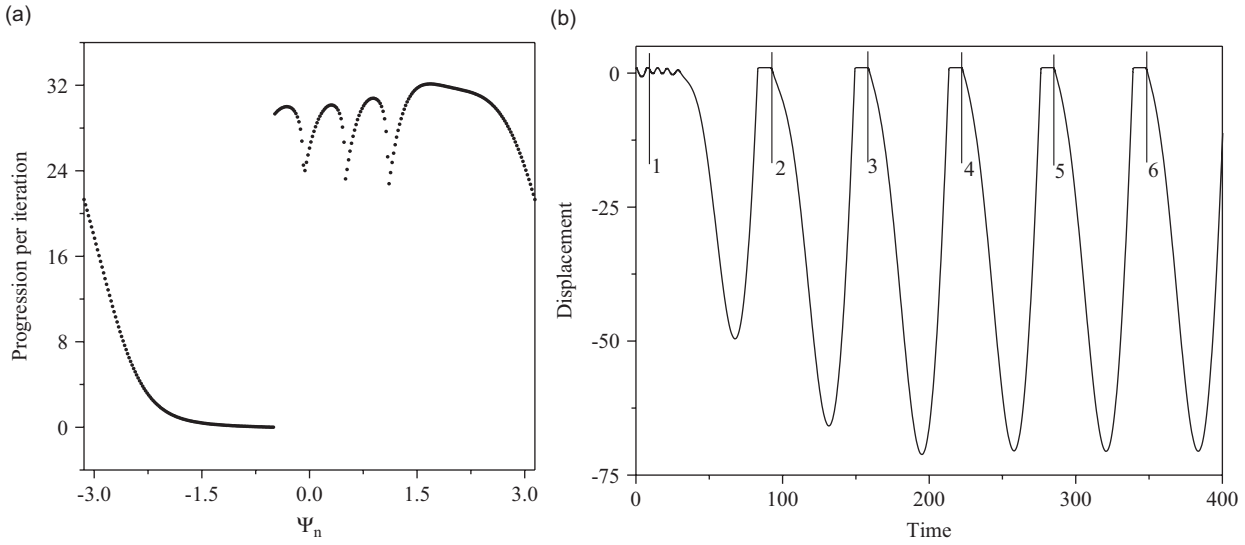

Fig. 10. (a) Progression as function of initial phase shift ψ_n and (b) time history for the iteration of the map shown in Fig. 7(a) at $a = 0.3$, $b = 0.15$, $\xi = 0.01$, $\omega = 0.1$, $\varphi = 0$, $g = 0.02$.

The practical application of the developed map is to determine a progression of a vibro-impact system (see [43]). The progression per one iteration of the map can be calculated using Eq. (5) and its dependance on the phase shift ψ_n is given in Fig. 10a. As can be seen from this figure the discontinuity of the map shown in Fig. 7a at $\psi_n = -0.499$ corresponds to the jump of the progression per iteration.

From the analysis given above the following conclusions could be drawn. First, the discontinuities of the 1D map are connected with grazing of the trajectory with hypersurface $\Pi\mathbf{X}_{2,3}$ (i.e. the mass hits the slider but not strong enough to make a progression), and this produces as a consequence a jump of progression per iteration at certain value of ψ_n, and second, the breaks of smoothness correspond to grazing of the trajectory with hypersurface $\Pi\mathbf{X}_{1,2}$, when the mass grazes the slider.

Comparisons of bifurcation diagrams calculated using the original differential equation Eqs. (2), 2D map and 1D approximate map are shown in Fig. 11, where varying system parameter is static force b. The diagrams presented in Figs. 11b and c are constructed by taking 300 iterations of the maps after eliminating the transient processes (first 100 points of the maps iterations), while the diagram presented in Fig. 11a is constructed by taking 300 points, once per period of external excitation, also after the transient process has died down (which is assumed to last for 100 periods). As can clearly be seen from this figure for the most values of the static force b, all diagrams indicate the same types of regimes. However, there are several values (for example, $b = 0.27$ marked by dash line) where the period two orbit shown in Figs. 11b and c appears as period one orbit in Fig. 11a. This is because the duration of one iteration of both 2D map and 1D approximate map is not constant, and for $b = 0.27$ during one period of external excitation the progression phase occurs twice.

6. Conclusions

Dynamics of the piecewise smooth nonlinear oscillators was considered, for which general methodology of reducing multidimensional flows to low-dimensional maps has been proposed. It is postulated that the idea developed in this paper is general and can be used for any piecewise smooth oscillator. To construct a low-dimensional map, it is proposed to monitor the points of intersections of a chosen boundary between smooth subspaces by a trajectory. The reduction of dimension is directly related to the dimension of the chosen hypersurface, and the lower its dimension is, the larger dimension reduction can be achieved. The general methodology includes a creation of the global map comprised of local maps constructed in the smooth sub-regions of phase space.

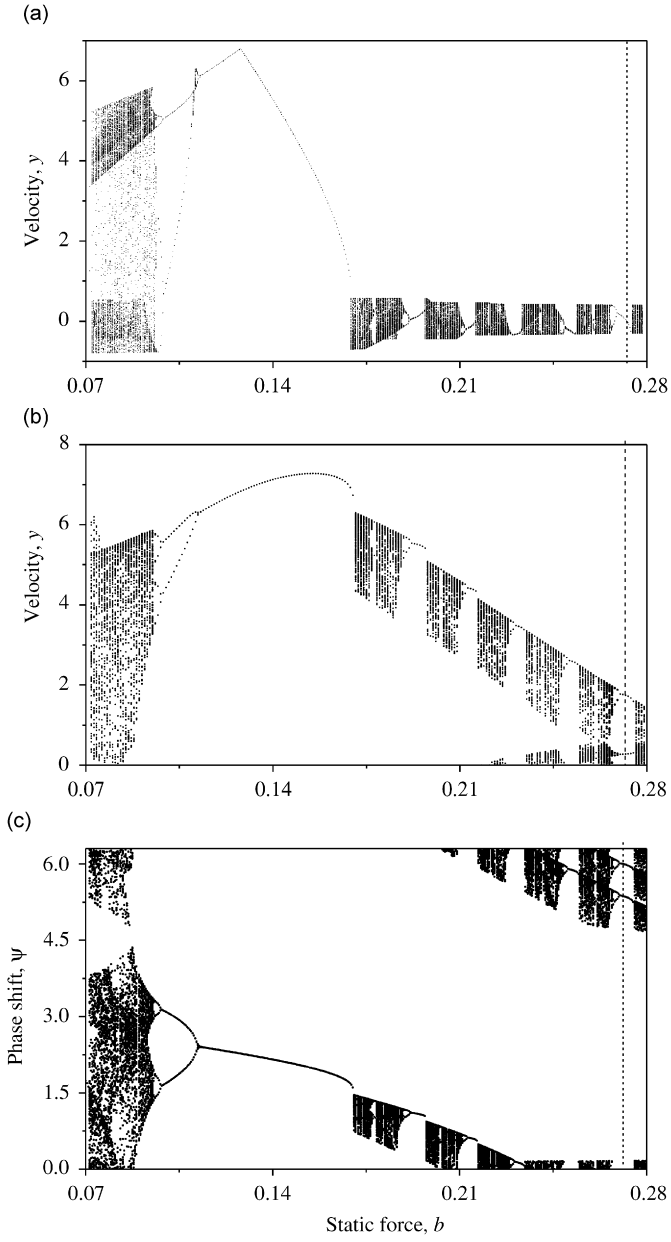

Fig. 11. Bifurcation diagrams $\psi(b)$ calculated for $a = 0.3$, $\xi = 0.01$, $\omega = 0.1$, $\varphi = \pi/2$, $g = 0.02$ using (a) original differential equations, (b) 2D map and (c) 1D approximate map.

Full details were given for a drifting impact oscillator, where 5D flow was reduced to 1D approximate analytical map. An exact 2D map has been formulated and analysed. A further reduction to 1D approximate map has been introduced and discussed. Piecewise smooth nature of the 2D and 1D approximate maps was discovered, and it was found that breaks of the smoothness is caused by de-phasing of the system which happens when trajectory grazes with hypersurfaces $\Pi\mathbf{X}_{1,2}$ and $\Pi\mathbf{X}_{2,3}$. Standard nonlinear dynamic analysis revealed complex behaviour ranging from periodic oscillations to chaos and co-existence of multiple attractors. Accuracy of the constructed maps was examined by comparing the dynamics responses with the exact solutions for a wide range of system parameters and showing a good correspondence of approximate and exact results.

The main advantage of the proposed methodology is a large potential gain in dimensionality reduction which translates to much faster and more accurate numerical analysis. This aspect will demonstrate its importance when designing a control system in practical application (e.g. vibro-impact moling, [43]). More work on so-called manifold reduction is required to generalize the proposed method to the smooth dynamical systems and to transform the implicit maps (e.g. Eq. (12)) to explicit ones. Such explicit maps would reduce the computational time even further.

Acknowledgement

The first author acknowledges the financial support from Nuffield Foundation and EPSRC.

Appendix A

The solutions for each phase are given below for system initial position $(\tau_0; p_0, y_0, q_0)$.
For *No Contact* phase:

$$\begin{aligned} p(\tau) &= p_0 + y_0(\tau-\tau_0) + \frac{b}{2}(\tau-\tau_0)^2 \\ &\quad - \frac{a}{\omega^2}[\cos(\omega\tau+\varphi) - \cos(\omega\tau_0+\varphi) + \omega(\tau-\tau_0)\sin(\omega\tau_0+\varphi)], \\ y(\tau) &= y_0 + b(\tau-\tau_0) + \frac{a}{\omega}[\sin(\omega\tau+\varphi) - \sin(\omega\tau_0+\varphi)], \\ q(\tau) &= q_0 \exp\left(-\frac{\tau-\tau_0}{2\xi}\right). \end{aligned} \tag{22}$$

For *Contact without progression* phase:

$$\begin{aligned} p(\tau) &= b + e + \exp(-\xi(\tau-\tau_0))\sqrt{C_1^2+C_2^2}\sin\left(\sqrt{1-\xi^2}(\tau-\tau_0) + \beta(C_1,C_2)\right) \\ &\quad + \frac{a}{\sqrt{(1-\omega^2)^2+4\xi^2\omega^2}}\sin(\omega\tau+\varphi+\alpha), \\ y(\tau) &= \exp(-\xi(\tau-\tau_0))\sqrt{C_1^2+C_2^2}\sin\left(\sqrt{1-\xi^2}(\tau-\tau_0) + \delta(C_1,C_2)\right) \\ &\quad + \frac{a\omega}{\sqrt{(1-\omega^2)^2+4\xi^2\omega^2}}\cos(\omega\tau+\varphi+\alpha), \\ q(\tau) &= b + \exp(-\xi(\tau-\tau_0))\sqrt{C_1^2+C_2^2}\sin\left(\sqrt{1-\xi^2}(\tau-\tau_0) + \beta(C_1,C_2)\right) \\ &\quad + \frac{a}{\sqrt{(1-\omega^2)^2+4\xi^2\omega^2}}\sin(\omega\tau+\varphi+\alpha), \end{aligned} \tag{23}$$

where

$$C_1(\tau_0, p_0) = p_0 - b - e - \frac{a}{\sqrt{(1-\omega^2)^2+4\xi^2\omega^2}}\sin(\omega\tau_0+\varphi+\alpha), \tag{24}$$

$$C_2(\tau_0, p_0, y_0) = \frac{1}{\sqrt{1-\xi^2}}\left\{ y_0 + \xi(p_0-b-e) - \frac{a\sqrt{\xi^2+\omega^2}}{\sqrt{(1-\omega^2)^2+4\xi^2\omega^2}}\sin(\omega\tau_0+\varphi+\alpha+\gamma) \right\} \tag{25}$$

and

$$\begin{aligned}\alpha &= \arctan\left(\frac{1-\omega^2}{2\xi\omega}\right),\\ \gamma &= \arctan\left(\frac{\omega}{\xi}\right),\\ \beta(C_1,C_2) &= \arctan\left(\frac{C_1}{C_2}\right),\\ \delta(C_1,C_2) &= \arctan\left(\frac{-\xi C_1+\sqrt{1-\xi^2}C_2}{-\sqrt{1-\xi^2}C_1-\xi C_2}\right).\end{aligned} \tag{26}$$

For *Contact with progression* phase:

$$\begin{aligned}p(\tau) &= e+1+(p_0-e-1)\exp\left(-\frac{\tau-\tau_0}{2\xi}\right),\\ y(\tau) &= y_0+(b-1)(\tau-\tau_0)+\frac{a}{\omega}[\sin(\omega\tau+\varphi)-\sin(\omega\tau_0+\varphi)],\\ q(\tau) &= 1+(q_0-1)\exp\left(-\frac{\tau-\tau_0}{2\xi}\right).\end{aligned} \tag{27}$$

Appendix B

The mapping $\mathbf{P}_2$ relates the initial moment of *Contact with progression* mode with its final moment. Equation $\mathscr{G}_2(\tau_{i+2}) = y(\tau_{i+2}) + p(\tau_{i+2}) - e - 1 = 0$ is another implicit equation which needs to be solved in order to determine time τ_{i+2}, when the second mapping is completed. Formulae for $y(\cdot)$ and $p(\cdot)$ are given in Eq. (27):

$$\begin{aligned}\mathscr{G}_2(\tau_{i+2}) = y_{i+1}&\left(1-\exp\left(-\frac{\tau_{i+2}-\tau_{i+1}}{2\xi}\right)\right)+(b-1)(\tau_{i+2}-\tau_{i+1})\\ &+\frac{a}{\omega}[\sin(\omega\tau_{i+2}+\varphi)-\sin(\omega\tau_{i+1}+\varphi)]=0.\end{aligned} \tag{28}$$

Once τ_{i+2} is calculated, the velocity y_{i+2} can be determined from

$$y_{i+2} = y_{i+1}+(b-1)(\tau_{i+2}-\tau_{i+1})+\frac{a}{\omega}[\sin(\omega\tau_{i+2}+\varphi)-\sin(\omega\tau_{i+1}+\varphi)]. \tag{29}$$

$\mathbf{P}_3$ associates the final moment of *Contact with progression* mode with the initial moment of *No contact* mode. To find τ_{i+3} yet again an implicit equation $\mathscr{G}_3(\tau_{i+3}) = 2\xi y(\tau_{i+3}) + p(\tau_{i+3}) - e = 0$ has to be solved, where functions $y(\cdot)$ and $p(\cdot)$ are given by Eq. (23). By substituting

$$\tau_{i+1} \to \tau_{i+3}, \quad \tau_i \to \tau_{i+2}, \quad y_i \to y_{i+2}$$

to Eq. (12) one shall arrive with

$$\mathscr{G}_3 = \mathscr{G}_1 + 1, \tag{30}$$

where coefficients C_1 and C_2 are now calculated as

$$\begin{aligned}C_1 &= C_1(\tau_{i+2}, 1+e-2\xi y_{i+2}),\\ C_2 &= C_2(\tau_{i+2}, 1+e-2\xi y_{i+2}, y_{i+2}).\end{aligned} \tag{31}$$

Once equation $\mathscr{G}_3 = 0$ is solved and the time τ_{i+3} is calculated, first velocity y_{i+3} and then relative displacement p_{i+3} can be determined from

$$y_{i+3} = \exp(-\xi(\tau_{i+3} - \tau_{i+2}))\sqrt{C_1^2 + C_2^2}\sin\left(\sqrt{1-\xi^2}(\tau_{i+3} - \tau_{i+2}) + \delta(C_1, C_2)\right) + \frac{a\omega}{\sqrt{(1-\omega^2)^2 + 4\xi^2\omega^2}}\cos(\omega\tau_{i+3} + \varphi + \alpha),$$

$$p_{i+3} = e - 2\xi y_{i+3}, \tag{32}$$

where coefficients $C_1,\ C_2$ are given in Eq. (31).

And finally the mapping $\mathbf{P}_4$ associates the initial moment of *No Contact* mode with its final moment. As before to find τ_{i+4} the equation $\mathscr{G}_4(\tau_{i+4}) = p(\tau_{i+4}) - q(\tau_{i+4}) - e = 0$ has to be solved, where functions $y(\cdot)$ and $p(\cdot)$ are given by Eq. (22):

$$\mathscr{G}_4(\tau_{i+4}) = e - 2\xi y_{i+3} + y_{i+3}(\tau_{i+4} - \tau_{i+3}) + \frac{b}{2}(\tau_{i+4} - \tau_{i+3})^2 - \frac{a}{\omega^2}[\cos(\omega\tau_{i+4} + \varphi) - \cos(\omega\tau_{i+3} + \varphi) + \omega(\tau_{i+4} - \tau_{i+3})\sin(\omega\tau_{i+3} + \varphi)] + 2\xi y_{i+3}\exp\left(-\frac{\tau_{i+4} - \tau_{i+3}}{2\xi}\right) - e = 0. \tag{33}$$

Once Eq. (33) is solved and τ_{i+4} is found, y_{i+4} can be calculated

$$y_{i+4} = y_{i+3} + b(\tau_{i+4} - \tau_{i+3}) + \frac{a}{\omega}[\sin(\omega\tau_{i+4} + \varphi) - \sin(\omega\tau_{i+3} + \varphi)]. \tag{34}$$

The mapping $\mathbf{P}_5$ associates the initial moment of *Contact without progression* mode (τ_i, y_i) with initial moment of *No contact* mode (τ_{i+1}, y_{i+1}). To find τ_{i+1} the equation $\mathscr{G}_5(\tau_{i+1}) = 0$ has to be solved, where $\mathscr{G}_5(\tau_{i+1}) = 2\xi y(\tau_{i+1}) + p(\tau_{i+1}) - e$ and functions $y(\cdot)$ and $p(\cdot)$ are again given by Eqs. (23). Thus

$$\mathscr{G}_5 = \mathscr{G}_1 + 1, \tag{35}$$

where coefficients C_1 and C_2 are calculated as (see Eqs. (26))

$$C_1 = C_1(\tau_i, e),$$
$$C_2 = C_2(\tau_i, e, y_i). \tag{36}$$

Once equation $\mathscr{G}_5(\tau_{i+1}) = 0$ is solved and τ_{i+1} is found, y_{i+1} and p_{i+1} are calculated from

$$y_{i+1} = \exp(-\xi(\tau_{i+1} - \tau_i))\sqrt{C_1^2 + C_2^2}\sin\left(\sqrt{1-\xi^2}(\tau_{i+1} - \tau_i) + \delta(C_1, C_2)\right) + \frac{a\omega}{\sqrt{(1-\omega^2)^2 + 4\xi^2\omega^2}}\cos(\omega\tau_{i+1} + \varphi + \alpha),$$

$$p_{i+1} = e - 2\xi y_{i+1}, \tag{37}$$

where coefficients $C_1,\ C_2$ are given in Eqs. (36).

The mapping $\mathbf{P}_6$ associates the final moment of *Contact with progression* mode (τ_i, y_i) with initial of *Contact with progression* mode (τ_{i+1}, y_{i+1}). To find τ_{i+1} equation $\mathscr{G}_6(\tau_{i+1}) = 0$, has to be solved, where $\mathscr{G}_6(\tau_{i+1}) = 2\xi y(\tau_{i+1}) + p(\tau_{i+1}) - e - 1$ and functions $y(\cdot)$ and $p(\cdot)$ are given by Eqs. (23). Thus

$$\mathscr{G}_6 = \mathscr{G}_1, \tag{38}$$

where coefficients C_1 and C_2 are calculated as (see Eqs. (26))

$$C_1 = C_1(\tau_i, 1 + e - 2\xi y_i),$$
$$C_2 = C_2(\tau_i, 1 + e - 2\xi y_i, y_i). \tag{39}$$

Once equation $\mathscr{G}_6(\tau_{i+1})=0$ is solved and τ_{i+1} is found, y_{i+1} and p_{i+1} can be determined from

$$\begin{aligned} y_{i+1} &= \exp(-\xi(\tau_{i+1}-\tau_i))\sqrt{C_1^2+C_2^2}\sin\left(\sqrt{1-\xi^2}(\tau_{i+1}-\tau_i)+\delta(C_1,C_2)\right) \\ &\quad + \frac{a\omega}{\sqrt{(1-\omega^2)^2+4\xi^2\omega^2}}\cos(\omega\tau_{i+1}+\varphi+\alpha), \\ p_{i+1} &= 1+e-2\xi y_{i+1}, \end{aligned} \tag{40}$$

where coefficients $C_1,\ C_2$ are given in Eqs. (39).

The results of calculation of partial differentials for each mode are given below.

For mapping $\mathbf{P}_1$ we obtain:

$$\begin{aligned} \frac{\partial \mathscr{G}_1}{\partial \tau_i} &= \exp(-\xi(\tau_{i+1}-\tau_i))\sqrt{C_1^2+C_2^2}\left\{\left(\xi+\frac{C_1\dfrac{\partial C_1}{\partial \tau_i}+C_2\dfrac{\partial C_2}{\partial \tau_i}}{C_1^2+C_2^2}\right)\right. \\ &\quad\times\left[2\xi\sin\left(\sqrt{1-\xi^2}(\tau_{i+1}-\tau_i)+\delta(C_1,C_2)\right)+\sin\left(\sqrt{1-\xi^2}(\tau_{i+1}-\tau_i)+\beta(C_1,C_2)\right)\right] \\ &\quad+\left(-\sqrt{1-\xi^2}+\frac{C_2\dfrac{\partial C_1}{\partial \tau_i}-C_1\dfrac{\partial C_2}{\partial \tau_i}}{C_1^2+C_2^2}\right) \\ &\quad\left.\times\left[2\xi\cos\left(\sqrt{1-\xi^2}(\tau_{i+1}-\tau_i)+\delta(C_1,C_2)\right)+\cos\left(\sqrt{1-\xi^2}(\tau_{i+1}-\tau_i)+\beta(C_1,C_2)\right)\right]\right\}, \end{aligned} \tag{41}$$

$$\begin{aligned} \frac{\partial \mathscr{G}_1}{\partial y_i} &= \frac{\exp(-\xi(\tau_{i+1}-\tau_i))}{\sqrt{C_1^2+C_2^2}}\left\{\left(C_1\frac{\partial C_1}{\partial y_i}+C_2\frac{\partial C_2}{\partial y_i}\right)\right. \\ &\quad\times\left[2\xi\sin(\sqrt{1-\xi^2}(\tau_{i+1}-\tau_i)+\delta(C_1,C_2))+\sin\left(\sqrt{1-\xi^2}(\tau_{i+1}-\tau_i)+\beta(C_1,C_2)\right)\right] \\ &\quad+\left(C_2\frac{\partial C_1}{\partial y_i}-C_1\frac{\partial C_2}{\partial y_i}\right) \\ &\quad\left.\times\left[2\xi\cos(\sqrt{1-\xi^2}(\tau_{i+1}-\tau_i)+\delta(C_1,C_2))+\cos\left(\sqrt{1-\xi^2}(\tau_{i+1}-\tau_i)+\beta(C_1,C_2)\right)\right]\right\}, \end{aligned} \tag{42}$$

$$\begin{aligned} \frac{\partial \mathscr{G}_1}{\partial \tau_{i+1}} &= \exp(-\xi(\tau_{i+1}-\tau_i))\sqrt{C_1^2+C_2^2}\left[2\xi\left(-\xi\sin\left(\sqrt{1-\xi^2}(\tau_{i+1}-\tau_i)+\delta(C_1,C_2)\right)\right.\right. \\ &\quad\left.+\sqrt{1-\xi^2}\cos\left(\sqrt{1-\xi^2}(\tau_{i+1}-\tau_i)+\delta(C_1,C_2)\right)\right)-\xi\sin\left(\sqrt{1-\xi^2}(\tau_{i+1}-\tau_i)+\beta(C_1,C_2)\right) \\ &\quad\left.+\sqrt{1-\xi^2}\cos\left(\sqrt{1-\xi^2}(\tau_{i+1}-\tau_i)+\beta(C_1,C_2)\right)\right] \\ &\quad+\frac{a\omega}{\sqrt{(1-\omega^2)^2+4\xi^2\omega^2}}[-2\xi\omega\sin(\omega\tau_{i+1}+\varphi+\alpha)+\cos(\omega\tau_{i+1}+\varphi+\alpha)]. \end{aligned} \tag{43}$$

Where coefficients C_1, C_2 are given in Eqs. (13) and

$$\frac{\partial C_1}{\partial \tau_i} = -\frac{a\omega}{\sqrt{(1-\omega^2)^2+4\xi^2\omega^2}}\cos(\omega\tau_i+\varphi+\alpha), \quad \frac{\partial C_1}{\partial y_i}=0,$$

$$\frac{\partial C_2}{\partial \tau_i} = -\frac{a\omega}{\sqrt{(1-\omega^2)^2+4\xi^2\omega^2}}\sqrt{\frac{\xi^2+\omega^2}{1-\xi^2}}\cos(\omega\tau_i+\varphi+\alpha+\gamma), \quad \frac{\partial C_2}{\partial y_i}=\frac{1}{\sqrt{1-\xi^2}}. \tag{44}$$

Thus we have

$$\frac{\partial \tau_{i+1}}{\partial \tau_i} = -\frac{\partial \mathscr{G}_1}{\partial \tau_i}\Big/\frac{\partial \mathscr{G}_1}{\partial \tau_{i+1}}, \tag{45}$$

$$\frac{\partial \tau_{i+1}}{\partial y_i} = -\frac{\partial \mathscr{G}_1}{\partial y_i}\Big/\frac{\partial \mathscr{G}_1}{\partial \tau_{i+1}}, \tag{46}$$

where $\partial\mathscr{G}_1/\partial\tau_i$, $\partial\mathscr{G}_1/\partial y_i$ and $\partial\mathscr{G}_1/\partial\tau_{i+1}$ ave given by Eqs. (41)–(43). Then we can calculate

$$\begin{aligned}\frac{\partial y_{i+1}}{\partial \tau_i} = {} & \exp(-\xi(\tau_{i+1}-\tau_i))\sqrt{C_1^2+C_2^2} \\ & \times\left\{\sin\left(\sqrt{1-\xi^2}(\tau_{i+1}-\tau_i)+\delta(C_1,C_2)\right)\left[-\xi\left(\frac{\partial\tau_{i+1}}{\partial\tau_i}-1\right)+\frac{C_1\frac{\partial C_1}{\partial\tau_i}+C_2\frac{\partial C_2}{\partial\tau_i}}{C_1^2+C_2^2}\right]\right. \\ & \left.+\cos\left(\sqrt{1-\xi^2}(\tau_{i+1}-\tau_i)+\delta(C_1,C_2)\right)\left[\sqrt{1-\xi^2}\left(\frac{\partial\tau_{i+1}}{\partial\tau_i}-1\right)+\frac{C_2\frac{\partial C_1}{\partial\tau_i}-C_1\frac{\partial C_2}{\partial\tau_i}}{C_1^2+C_2^2}\right]\right\} \\ & -\frac{a\omega^2}{\sqrt{(1-\omega^2)^2+4\xi^2\omega^2}}\sin(\omega\tau_{i+1}+\varphi+\alpha)\frac{\partial\tau_{i+1}}{\partial\tau_i},\end{aligned} \tag{47}$$

$$\begin{aligned}\frac{\partial y_{i+1}}{\partial y_i} = {} & \exp(-\xi(\tau_{i+1}-\tau_i))\sqrt{C_1^2+C_2^2} \\ & \times\left\{\sin\left(\sqrt{1-\xi^2}(\tau_{i+1}-\tau_i)+\delta(C_1,C_2)\right)\left[-\xi\frac{\partial\tau_{i+1}}{\partial y_i}+\frac{C_1\frac{\partial C_1}{\partial y_i}+C_2\frac{\partial C_2}{\partial y_i}}{C_1^2+C_2^2}\right]\right. \\ & \left.+\cos\left(\sqrt{1-\xi^2}(\tau_{i+1}-\tau_i)+\delta(C_1,C_2)\right)\left[\sqrt{1-\xi^2}\frac{\partial\tau_{i+1}}{\partial y_i}+\frac{C_2\frac{\partial C_1}{\partial y_i}-C_1\frac{\partial C_2}{\partial y_i}}{C_1^2+C_2^2}\right]\right\} \\ & -\frac{a\omega^2}{\sqrt{(1-\omega^2)^2+4\xi^2\omega^2}}\sin(\omega\tau_{i+1}+\varphi+\alpha)\frac{\partial\tau_{i+1}}{\partial y_i},\end{aligned} \tag{48}$$

where $(\partial\tau_{i+1})/\partial\tau_i$ and $(\partial\tau_{i+1})/\partial y_i$ are given by Eqs. (45)–(46).

For mapping $\mathbf{P}_2$ it has been obtained

$$\frac{\partial\tau_{i+2}}{\partial y_{i+1}} = \frac{\exp\left(-\frac{\tau_{i+2}-\tau_{i+1}}{2\xi}\right)-1}{b-1+a\cos(\omega\tau_{i+2}+\varphi)+\frac{y_{i+1}}{2\xi}\exp\left(-\frac{\tau_{i+2}-\tau_{i+1}}{2\xi}\right)}, \tag{49}$$

$$\frac{\partial\tau_{i+2}}{\partial\tau_{i+1}}=\frac{b-1+a\cos(\omega\tau_{i+1}+\varphi)+\dfrac{y_{i+1}}{2\xi}\exp\left(-\dfrac{\tau_{i+2}-\tau_{i+1}}{2\xi}\right)}{b-1+a\cos(\omega\tau_{i+2}+\varphi)+\dfrac{y_{i+1}}{2\xi}\exp\left(-\dfrac{\tau_{i+2}-\tau_{i+1}}{2\xi}\right)}, \tag{50}$$

$$\frac{\partial y_{i+2}}{\partial y_{i+1}}=1+(b-1+a\cos(\omega\tau_{i+2}+\varphi))\frac{\partial\tau_{i+2}}{\partial y_{i+1}}, \tag{51}$$

$$\frac{\partial y_{i+2}}{\partial\tau_{i+1}}=(b-1)\left[\frac{\partial\tau_{i+2}}{\partial\tau_{i+1}}-1\right]+a\left(\cos(\omega\tau_{i+2}+\varphi)\frac{\partial\tau_{i+2}}{\partial\tau_{i+1}}-\cos(\omega\tau_{i+1}+\varphi)\right). \tag{52}$$

For mapping $\mathbf{P}_3$ we have $\mathscr{G}_3=\mathscr{G}_1+1$, where one have to substitute

$$\tau_{i+1}\to\tau_{i+3},\quad \tau_i\to\tau_{i+2},\quad y_i\to y_{i+2},\quad y_{i+1}\to y_{i+3}.$$

With this substitution formulas (41)–(43) and (45)–(48) can be used keeping in mind that C_1 and C_2 are now given by Eqs. (31) and

$$\frac{\partial C_1}{\partial\tau_i}=-\frac{a\omega}{\sqrt{(1-\omega^2)^2+4\xi^2\omega^2}}\cos(\omega\tau_i+\varphi+\alpha),\quad \frac{\partial C_1}{\partial y_i}=-2\xi,$$

$$\frac{\partial C_2}{\partial\tau_i}=-\frac{a\omega}{\sqrt{(1-\omega^2)^2+4\xi^2\omega^2}}\sqrt{\frac{\xi^2+\omega^2}{1-\xi^2}}\cos(\omega\tau_i+\varphi+\alpha+\gamma),\quad \frac{\partial C_2}{\partial y_i}=\frac{1-2\xi^2}{\sqrt{1-\xi^2}}. \tag{53}$$

For mapping $\mathbf{P}_4$ it has been obtained

$$\frac{\partial\tau_{i+4}}{\partial y_{i+3}}=\frac{2\xi\left(1-\exp\left(-\dfrac{\tau_{i+4}-\tau_{i+3}}{2\xi}\right)\right)+(\tau_{i+4}-\tau_{i+3})}{y_{i+3}\left(1-\exp\left(-\dfrac{\tau_{i+4}-\tau_{i+3}}{2\xi}\right)\right)+b(\tau_{i+4}-\tau_{i+3})+\dfrac{a}{\omega}(\sin(\omega\tau_{i+4}+\varphi)-\sin(\omega\tau_{i+3}+\varphi))}, \tag{54}$$

$$\frac{\partial\tau_{i+4}}{\partial\tau_{i+3}}=\frac{y_{i+3}\left(1-\exp\left(-\dfrac{\tau_{i+4}-\tau_{i+3}}{2\xi}\right)\right)+[b+\cos(\omega\tau_{i+3}+\varphi)](\tau_{i+4}-\tau_{i+3})}{y_{i+3}\left(1-\exp\left(-\dfrac{\tau_{i+4}-\tau_{i+3}}{2\xi}\right)\right)+b(\tau_{i+4}-\tau_{i+3})+\dfrac{a}{\omega}(\sin(\omega\tau_{i+4}+\varphi)-\sin(\omega\tau_{i+3}+\varphi))}, \tag{55}$$

$$\frac{\partial y_{i+4}}{\partial y_{i+3}}=1+[b+\cos(\omega\tau_{i+4}+\varphi)]\frac{\partial\tau_{i+4}}{\partial y_{i+3}}, \tag{56}$$

$$\frac{\partial y_{i+4}}{\partial\tau_{i+3}}=[b+\cos(\omega\tau_{i+4}+\varphi)]\frac{\partial\tau_{i+4}}{\partial\tau_{i+3}}-[b+\cos(\omega\tau_{i+3}+\varphi)]. \tag{57}$$

For mapping $\mathbf{P}_5$ associating the initial state of *Contact without progression* mode (τ_i,y_i) with initial state of *No contact* mode (τ_{i+1},y_{i+1}), we have $\mathscr{G}_5=\mathscr{G}_1+1$. Substituting $\mathscr{G}_1\to\mathscr{G}_5$, formulas (41)–(43) and (45)–(48) can be used keeping in mind that C_1 and C_2 are now given by Eqs. (36) and their partial differentials are given by Eqs. (44).

For mapping $\mathbf{P}_6$ associating the final state of *Contact with progression* mode (τ_i,y_i) with initial state of *Contact with progression* mode (τ_{i+1},y_{i+1}), we have $\mathscr{G}_6=\mathscr{G}_1$. Substituting $\mathscr{G}_1\to\mathscr{G}_6$, formulas (41)–(43) and (45)–(48) can be used keeping in mind that C_1 and C_2 are now given by Eqs. (39) and their partial differentials are given by Eqs. (53).

References

[1] S.J. Hogan, Heteroclinic bifurcations in damped rigid block motion, *Proceedings of the Royal Society of London: Part A* 439 (1992) 155–162.

[2] A.B. Nordmark, Non-periodic motion caused by grazing incidence in an impact oscillator, *Journal of Sound and Vibration* 145 (1991) 279–297.

[3] W. Chin, E. Ott, H.E. Nusse, C. Grebogi, Grazing bifurcations in impact oscillators, *Physical Review E* 50 (1994) 4427–4444.

[4] M. di Bernardo, M.I. Feigin, S.J. Hogan, M.E. Homer, Local analysis of C-bifurcations in *n*-dimensional piecewise smooth dynamical system, *Chaos, Solitons and Fractals* 10 (11) (1999) 1881–1908.

[5] C. Budd, F. Dux, Chattering and related behaviour in impact oscillators, *Philosophical Transactions of the Royal Society of London: Part A* 347 (1994) 365–389.

[6] M. di Bernardo, P. Kowalczyk, A. Nordmark, Bifurcations of dynamical systems with sliding: derivation of normal-form mapping, *Physica D* 170 (2002) 175–205.

[7] H. Dankowicz, A. Nordmark, On the origin and bifurcations of stick-slip oscillations, *Physica D* 136 (2000) 280–302.

[8] M. di Bernardo, C.J. Budd, A.R. Champneys, Normal-form maps for grazing bifurcations in *n*-dimensional piecewise smooth dynamical systems, *Physica D* 160 (2001) 222–254.

[9] H.E. Nusse, J.A. Yorke, Border-collision bifurcations including period two to period three for piecewise smooth systems, *Physica D* 57 (1992) 39–57.

[10] S. Banerjee, C. Grebogi, Border collision bifurcations in two-dimensional piecewise smooth maps, *Physical Review E* 59 (1999) 4052–4061.

[11] S. Banerjee, E. Ott, J.A. Yorke, G.H. Yuan, Anomalous bifurcations in DC-DC converters: boderline collisions in piecewise smooth maps, *Power Electronics Specialists, Conference*, 1997, pp. 1337–1344.

[12] S. Banerjee, K. Chakrabarty, Nonlinear modelling and bifurcations in the boost converter, *IEEE Transactions on Power Electronics* 13 (2) (1998) 252–260.

[13] U. Galvanetto, Bifurcations and chaos in a four dimensional mechanical system with dry friction, *Journal of Sound and Vibration* 204 (1997) 690–695.

[14] F. Peterka, J. Vacik, Transition to chaotic motion in mechanical systems with impacts, *Journal of Sound and Vibration* 154 (1) (1992) 95–115.

[15] S.W. Shaw, P.J. Holmes, A periodically forced piecewise linear oscillator, *Journal of Sound and Vibration* 90 (1) (1983) 129–155.

[16] S. Natsiavas, Periodic response and stability of oscillators with symmetric trilinear restoring force, *Journal of Sound and Vibration* 134 (2) (1989) 313–331.

[17] M. Wiercigroch, W.T.V. Sin, K. Li, Measurement of chaotic vibration in symmetrically piecewise linear oscillator, *Chaos, Solitons and Fractals* 9 (1–2) (1998) 209–220.

[18] E. Pavlovskaia, M. Wiercigroch, C. Grebogi, Modeling of an impact system with a drift, *Physical Review E* 64 (2001) 056224.

[19] K. Wiesenfeld, N.B. Tufillaro, Suppression of period doubling in the dynamics of a bouncing ball, *Physica D* 26 (1987) 321–335.

[20] H.D. Gonsalves, R.D. Neilson, A.D.S. Barr, A study of the response of a discontinuously nonlinear rotor system, *Nonlinear Dynamics* 7 (1995) 451–470.

[21] E. Karpenko, M. Wiercigroch, E.E. Pavlovskaia, M.P. Cartmell, Piecewise approximate solutions for a Jeffcott rotor with a snubber ring, *International Journal of Mechanical Sciences* 44 (2002) 475–488.

[22] E. Pavlovskaia, E.V. Karpenko, M. Wiercigroch, Nonlinear dynamic interactions of a Jeffcott rotor with a preloaded snubber ring, *Journal of Sound and Vibration* 276 (2004) 361–379.

[23] B. Feeny, A non-smooth Coulomb friction oscillator, *Physica D* 59 (1992) 25–38.

[24] M. Wiercigroch, Comments on the study of a harmonically excited linear oscillator with a Coulomb damper, *Journal of Sound and Vibration* 167 (1993) 560–563.

[25] A. Kahraman, R. Singh, Non-linear dynamics of a spur gear pair, *Journal of Sound and Vibration* 142 (1) (1990) 49–75.

[26] G. Litak, M.I. Friswell, Dynamics of a gear system with faults in meshing stiffness, *Nonlinear Dynamics* 41 (4) (2005) 415–421.

[27] S. Ebrahimi, P. Eberhard, Rigid-elastic modeling of meshing gear wheels in multibody systems, *Multibody System Dynamics* 16 (1) (2006) 55–71.

[28] I. Grabec, Chaotic dynamics of the cutting process, *International Journal of Machine Tools and Manufacture* 28 (1988) 19–32.

[29] M. Wiercigroch, Chaotic vibrations of a simple model of the machine tool-cutting process system, *Transactions of the ASME, Journal of Vibration and Acoustics* 119 (3) (1997) 468–475.

[30] A.F. Filippov, Differential equations with discontinuous right-hand side, *American Mathematical Society Translations* 42 (2) (1978) 199–231.

[31] M. Wiercigroch, B. de Kraker, (Eds.), *Applied Nonlinear Dynamics and Chaos of Mechanical Systems with Discontinuities*, Nonlinear Science Series A Vol. 28. World Scientific, Singapore, 2000.

[32] M. Kunze, *Non-Smooth Dynamical Systems*, Springer, Berlin, Heidelberg, New York, 2000.

[33] E. Pavlovskaia, M. Wiercigroch, Periodic solutions finder for vibro-impact oscillator with a drift, *Journal of Sound and Vibration* 267 (2003) 893–911.

[34] E. Pavlovskaia, M. Wiercigroch, Analytical drift reconstruction for impact oscillator with drift, *Chaos, Solitons and Fractals* 19 (1) (2004) 151–161.

[35] E. Pavlovskaia, M. Wiercigroch, C. Grebogi, Two dimensional map for impact oscillator with drift, *Physical Review E* 70 (2004) 036201.
[36] F. Peterka, Laws of impact motion of mechanical systems with one degree of freedom, part I—theoretical analysis of n-multiple $(1/n)$-impact motions, *Acta Technica ČSAV* 4 (1974) 462–473.
[37] F. Peterka, Laws of impact motion of mechanical systems with one degree of freedom, part II—results of analogue computer modelling of the motion, *Acta Technica ČSAV* 5 (1974) 569–580.
[38] G.S. Whiston, Global dynamics of a vibro-impacting linear oscillator, *Journal of Sound and Vibration* 118 (3) (1987) 395–429.
[39] G.S. Whiston, Singularities in vibro-impact dynamics, *Journal of Sound and Vibration* 152 (3) (1992) 427–460.
[40] E.N. Lorenz, Deterministic nonperiodic flow, *Journal of the Atmospheric Sciences* 20 (1963) 130.
[41] K. Ikeda, Multiple-valued stationary state and its instability of the transmitted light by a ring cavity system, *Optics Communications* 30 (1979) 257–261.
[42] A.C.J. Luo, S. Menon, Global chaos in a periodically forced, linear system with a dead-zone restoring force, *Chaos, Solitons and Fractals* 19 (5) (2004) 1189–1199.
[43] E.E. Pavlovskaia, M. Wiercigroch, K.-C. Woo, A.A. Rodger, Modelling of ground moling dynamics by an impact oscillator with a frictional slider, *Meccanica* 38 (2003) 85–97.